Hindawi
Advances in Materials Science and Engineering
Volume 2022, Article ID 9808782, 17 pages
https://doi.org/10.1155/2022/9808782

Research Article

Research on the Creep and Fatigue Evaluation Method of the Double-Layered Annulus Metal Hydride Bed Combined with Numerical Modeling and ASME Code

Ping Zhao, XiangGuo Zeng, Huayan Chen, and Xiuming Zhang

Key Laboratory of Deep Underground Science and Engineering (Ministry of Education), School of Architecture and Environment, Sichuan University, Chengdu 610065, China

Correspondence should be addressed to XiangGuo Zeng; xiangguozeng@scu.edu.cn and Huayan Chen; kay_chy@126.com

Received 11 August 2022; Revised 9 November 2022; Accepted 6 December 2022; Published 28 December 2022

Academic Editor: Marco Cannas

Applied to a hydrogen absorption-desorption cycle, the hydrogen storage bed will experience higher exchange temperatures and variety of mechanical load. Due to the complex structure of the double-layered annulus metal hydride bed and the importance of thermal stress on the failure of a metal hydride bed, the numerical modeling of its hot spot stress was carefully carried out. Moreover, in this paper, an analysis method considering the limit failure mode condition is proposed to deal with the stress analysis in the process of hydrogen absorption and desorption. According to the proposed analysis method, the maximum stress of thermal-structural coupling in the process of hydrogen absorption occurs at about 1/3 along the diameter direction and at the geometric mutation of the connection between the cooling pipe and the main body of the hydrogen storage bed in the process of hydrogen desorption. Apart from that, the hydrogen storage bed is also subjected to thermal-mechanical fatigue by the iterative process of absorption and desorption, and its operating temperature range is in the thermal creep temperature region. Based on the distribution of the stress and temperature, evaluation hot sites were selected and the ASME-NB and ASME-NH codes were used to evaluate fatigue and fatigue creep, respectively. The evaluation showed that the fatigue damage generated during its service life is small, while the creep damage is relatively large and the total damage generated during the service life of the hydrogen storage bed is within the safe range. Aiming at the structure and complex process of a double-layer hydrogen storage bed, creep and fatigue evaluation methods are proposed, various failure modes of hydrogen storage bed are highlighted, and the relationship between process parameters and life is established.

1. Introduction

As a clean, efficient and renewable energy vector, hydrogen energy has attracted much attention; however, the storage and safety of hydrogen energy are the most important factors preventing its widespread use [1]. Therefore, it is necessary to develop a hydrogen storage structure with high hydrogen storage efficiency and high strength. As a safe way to achieve rapid storage and supply of hydrogen isotopes, hydrogen storage beds are an important part of hydrogen storage systems [2]. This device contains the hydrogen storage material in a container of a certain structure and size, and the hydrogen storage material can absorb and desorb the hydrogen isotopes to complete the absorption and desorption of hydrogen isotopes [3]. In order to improve the charge-discharge efficiency, the cooling system is turned on in the hydrogen absorption process to take away the heat in time and to add heat to improve the reaction efficiency during the hydrogen desorption process [4]. During this period, the hydrogen storage bed is not only subjected to the thermal cycle load but also accompanied by the hydrogen pressure and the expansion and contraction pressure caused by the charging and discharging deformation of the hydrogen storage alloy [5]. This can cause thermal shock and stress concentrations in the hydrogen storage bed structure. With the increase of the number of hydrogen adsorption and desorption cycles, the continuous accumulation of stress and the increase of temperature duration may lead to thermal

creep and fracture failure of the hydrogen storage bed [6, 7]. So, it is critical to have a deep understanding of the complex stress phenomenon caused by the hydrogen absorption and release process.

Heubner et al. found that gas pressure, temperature, and metal hydride geometry all have an effect on stress evolution [8]. Once the elastic deformation of the reactor occurred during the hydriding-dehydriding cycles, its deformation did not become larger anymore [5]; however, after the plastic deformation of the reactor, the stress continued to increase and the stress increased with each cycle [9]. Ao et al. [10] studied the relationship between the wall stress of LaNi5 hydrogen storage bed and the cycle number of hydrogen adsorption-desorption cycles, loading of hydride bed, packing fraction, and thickness of bed's walls, and the results indicated that the wall stress increased with increasing packing fraction and decreased with thickening of the wall. Moreover, different locations exhibit vastly different maximum strain levels. Dinachandran and Mohan [11] used LaNi5 as a hydrogen storage alloy to numerically simulate the wall strain distribution of a vertically placed hydrogen storage device. The results showed that for a given charging rate, higher supply pressure and low coolant temperature were associated with higher wall strain rates. Most of the research on metal hydride hydrogen storage reactors is more focused on the hydrogen metal deformation of the hydrogen storage layer; however, it is rare for the stress characteristics investigation and safety assessments of solid-state hydrogen storage vessels in the process of hydrogen absorption-desorption. A design by the analysis approach was introduced which highlights detailed design procedures utilizing the results from stress analysis to evaluate components for plastic collapse, local failure, buckling, and cyclic loading. Due to the difficulty of experimental measurement and the high economic and time cost, the experimental method is not very suitable, but the numerical simulation method solves these problems well and is widely used in the field of structural analysis [12–14]. Therefore, the numerical simulation method is a favorable means to analyze the stress characteristics of hydrogen storage beds and to assist the safety assessment.

This paper emphasizes the analysis approach for fatigue, and the creep assessment of design is used to predict the lifetime of hydrogen storage bed which is subjected to cycles like hydrogen absorption and desorption process [15]. Hydrogen storage bed is inherently subjected to cyclic loads of pressure and temperature. Equivalent stresses and lifetime are evaluated by thermostructural analysis complying with the ASME code. The effect of different operating parameters on the equivalent stress peak value of the main body of the hydrogen storage bed was analyzed. Considering the ultimate failure mode of the hydrogen storage bed in the process of hydrogen absorption and desorption, the thermal fatigue and creep assessment was carried out.

2. Analysis Method and Evaluation Procedure

The overall analysis method flow of this work is shown in Figure 1. This process demonstrates the need for an analysis of the hydrogen storage bed's operating conditions and possible failure modes, followed by a thermal-structural analysis. In the thermal-structural coupling analysis, the interaction between the temperature field and the stress field needs to be considered, mainly including direct coupling and indirect coupling methods [16, 17]. If the final result does not satisfy the relevant criteria, it is necessary to modify the relevant parameters of the hydrogen storage bed according to the analysis of stress influencing factors and repeat the abovementioned steps until they are satisfied.

In the process of hydrogen absorption and desorption in the hydrogen storage bed, many factors such as the temperature drop rate and temperature rise rate of the hydrogen storage layer may lead to the destruction of the structure of the hydrogen storage bed. Many studies have shown that the structural damage is mainly caused by plastic yielding. Plastic yielding is the main cause of structural damage in hydrogen storage beds. In order to ensure the safety of the hydrogen storage bed structure in the process of hydrogen absorption and desorption, it is necessary to evaluate whether the stress of the hydrogen storage bed is greater than the allowable stress or not. The Von Mises yield criterion in many investigations [18, 19] has been used to assess whether a structure has undergone plastic yield failure or not. Judging from the joint cracking evaluation criteria, the initial cracking position of the hydrogen storage bed occurs at the location where the peak value of equivalent stress occurs. Therefore, this work studies the effect of the relevant parameters for the peak value of equivalent stress on the structure of the hydrogen storage bed during the hydrogen absorption and desorption process.

The evaluation rules of metal structures are divided into ASME-NB [20] and ASME-NH [21] according to whether the temperature is in the metal creep temperature range. Figure 2 shows the specific process and rules of structural integrity assessment.

From the description of the ASME-NB rules, the design condition, C-level condition, and D-level condition do not involve transient calculation; only one stress assessment is required, while for A- and B-level working conditions, thermal transients and pressure transients are often involved, so it is necessary to evaluate the strength range of primary and secondary stress and the cumulative service factor of fatigue.

While the hydrogen storage bed made of 316L stainless steel was subjected the high temperature and complex loading conditions, some failure modes, such as creep-fatigue damage, cyclic creep ratcheting, and excessive deformation over time should be considered [22, 23]. ASME Part III provides the design criteria for evaluating the integrity of structural components requiring load-controlled stress, deformation, strain, and creep-fatigue to meet the rules of the ASME code [14, 24, 25].

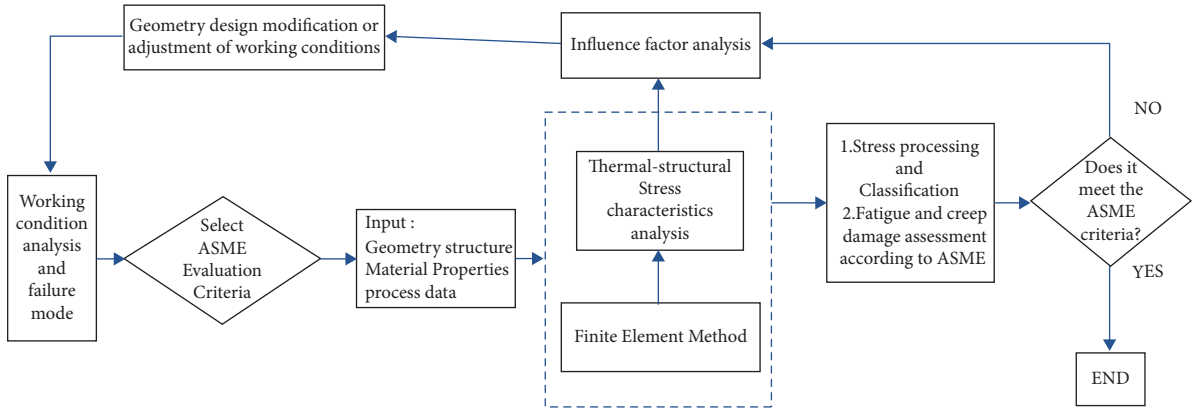

Figure 1: Analysis method flow chart.

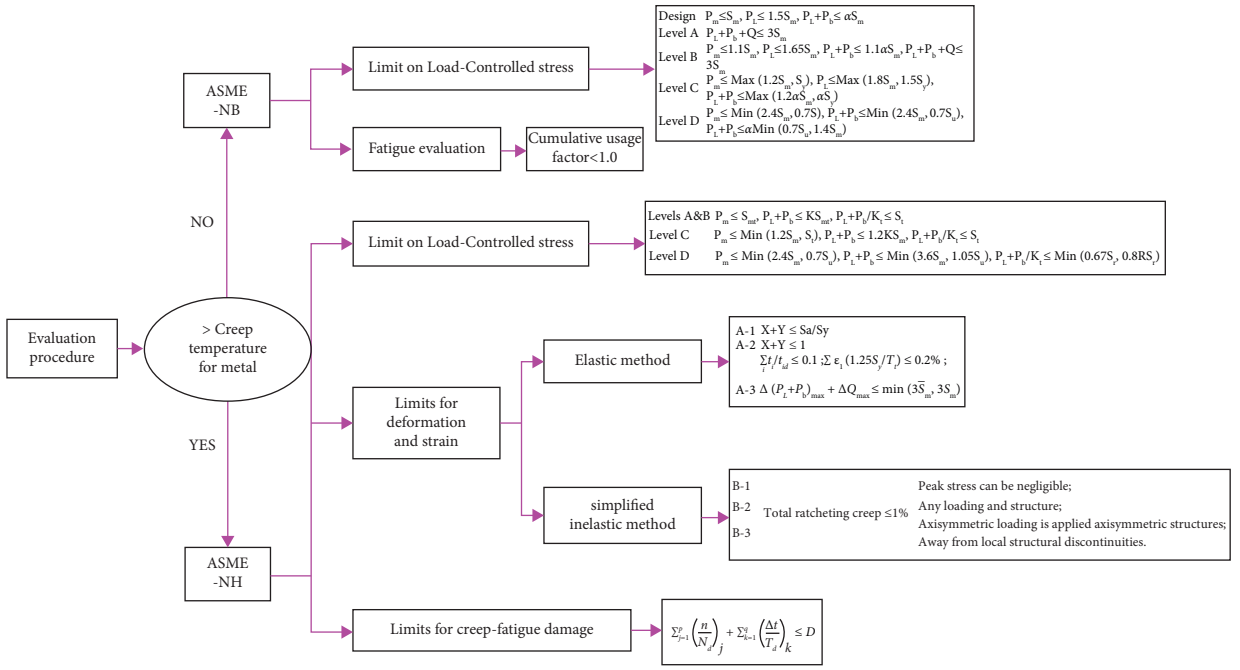

Figure 2: Creep and fatigue assessment procedure for the double-layered annulus metal hydride bed based on ASME code.

$$\Delta\varepsilon_{xi} = \varepsilon_{xi} - \varepsilon_{x0},$$

$$\Delta\varepsilon_{yi} = \varepsilon_{yi} - \varepsilon_{y0},$$

$$\Delta\varepsilon_{\text{equi},i} = \frac{\sqrt{2}}{2\left(1+\nu^{*}\right)}\left[\begin{array}{l}\left(\Delta\varepsilon_{xi}-\Delta\varepsilon_{yi}\right)^{2}+\\ \left(\Delta\varepsilon_{yi}-\Delta\varepsilon_{zi}\right)^{2}+\\ \left(\Delta\varepsilon_{zi}-\Delta\varepsilon_{xi}\right)^{2}+\\ \frac{3}{2}\left(\Delta\varepsilon_{xyi}+\Delta\varepsilon_{yzi}+\Delta\varepsilon_{zxi}\right)^{2}\end{array}\right]^{1/2}, \quad (1)$$

$$\Delta\varepsilon_{\max} = \operatorname{Max}\left(\Delta\varepsilon_{\text{equi},i}\right).$$

The total strain amplitude ε_t corresponding to the design fatigue curve was then determined by the following equation:

$$\varepsilon_t = K_v\Delta\varepsilon_{\text{mod}} + K\Delta\varepsilon_c, \quad (2)$$

$$\Delta\varepsilon_{\text{mod}} = K_e K\Delta\varepsilon_{\max}. \quad (3)$$

if $K\Delta\varepsilon_{\max} \le 3\overline{S}_m/E$, then $K_e = 1$; if $K\Delta\varepsilon_{\max} \ge 3\overline{S}_m/E$, then $K_e = K\Delta\varepsilon_{\max}E/3\overline{S}_m$.

$$K_v = 1.0 + f\left(K_v' - 1.0\right), \quad (4)$$

where the value is not less than 1, K_v' is the plastic Poisson's ratio adjustment coefficient, which can be obtained from Figure 3 [21]; f is the coefficient determined by the triaxial coefficient, which can be obtained from Figure 4 [21].

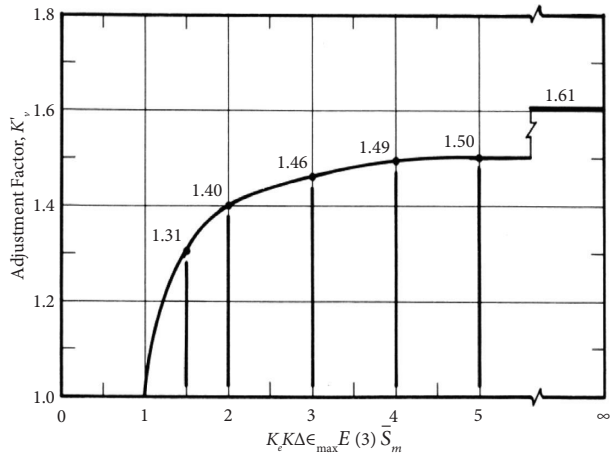

Figure 3: Adjustment for inelastic biaxial Poisson's ratio.

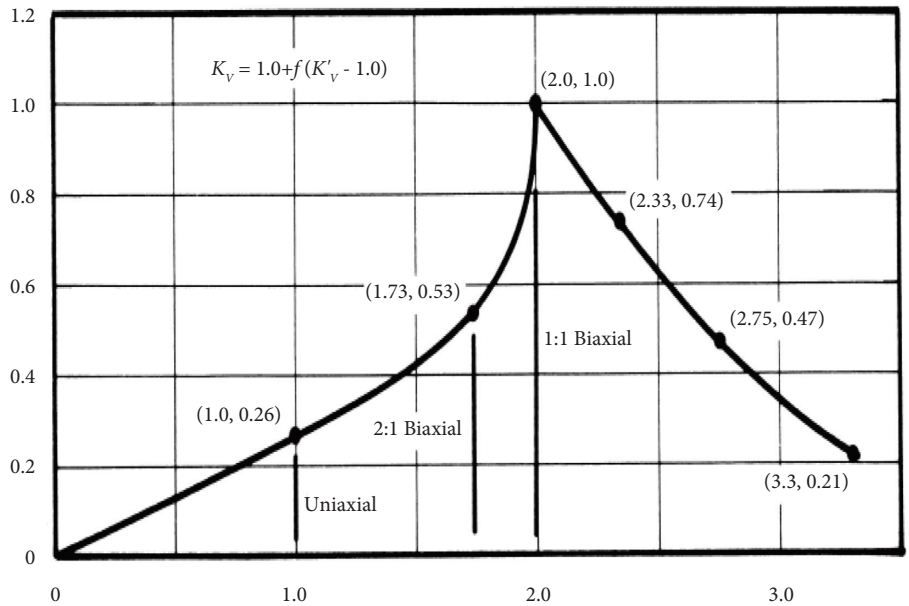

$$\text{T.F.} = \frac{|\sigma_1 + \sigma_2 + \sigma_3|}{\frac{1}{\sqrt{2}}\left[(\sigma_1 - \sigma_2)^2 + (\sigma_2 - \sigma_3)^2 + (\sigma_3 - \sigma_1)^2\right]1/2}$$

$\sigma's$ are principal stresses at extreme of stress cycle.

Figure 4: Inelastic multiaxial adjustments.

For inelastic analysis, ASME-NH provides a simplified method. The limits are required to satisfy any one of tests. The effective creep stress $\sigma_c = Z \bullet S_{yL}$ is determined by the primary and secondary stresses obtained from linear elastic stress analysis. Z is obtained by the Bree Diagram [26] with stress parameters X and Y, which can be calculated by equations (5) and (6):

$$X = \frac{(P_L + P_b/K_t)}{S_y}, \tag{5}$$

$$Y = \frac{(Q_R)_{\max}}{S_y}. \tag{6}$$

The Z corresponding to Tests B-1 and B-3 is determined by Figure 5 [27]. The equations defining the boundaries of the regimes P, $S1$, and $S2$.

In regimes S2, P, Z can be obtaine as

$$Z = X \cdot Y. \tag{7}$$

In regimes S_1, and

$$Z = Y + 1 - 2\sqrt{(1 - X)Y}. \tag{8}$$

In regimes E, $Z = X$.

The Z of Test No. B-2 is determined by Figure 6 [27].

The creep ratchet strain $\Delta\varepsilon_c$ corresponding to 1.25 σ_c is shown in Figure 7 [27].

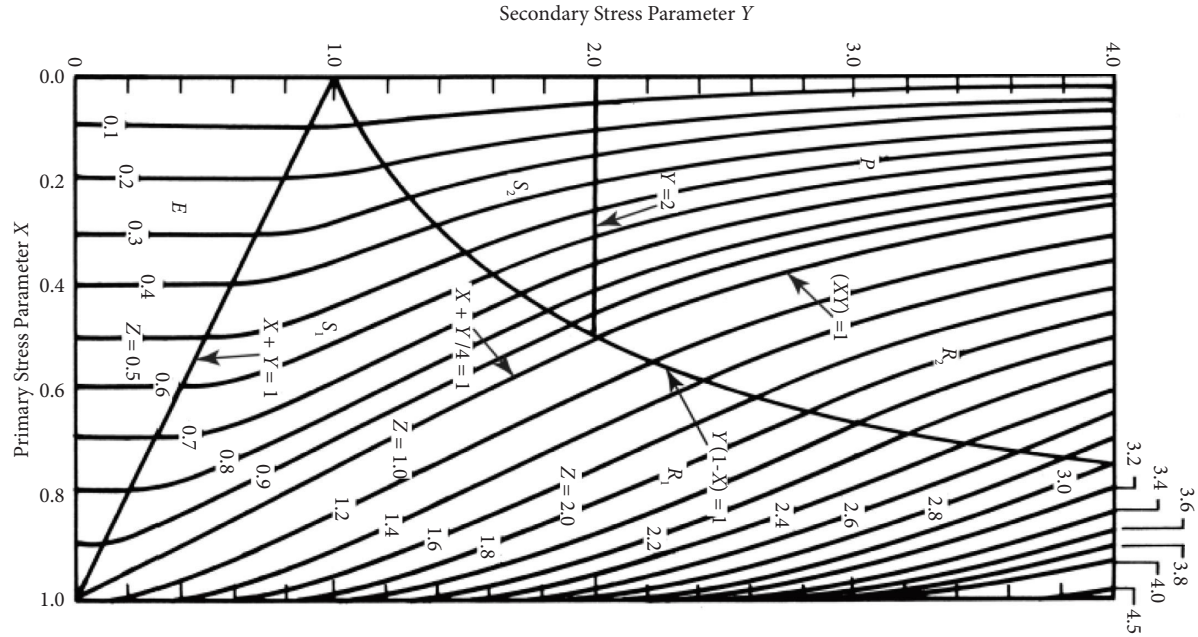

Figure 5: Effective creep stress parameter Z for simplified inelastic analysis using Test Nos. B-1 and B-3.

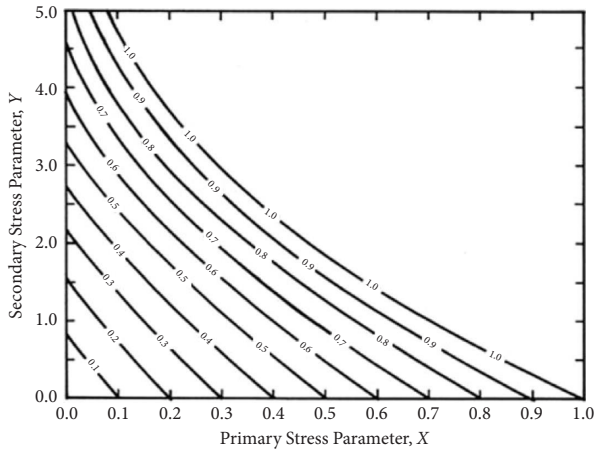

Figure 6: Effective creep stress parameter Z for simplified inelastic analysis using Test No. B-2.

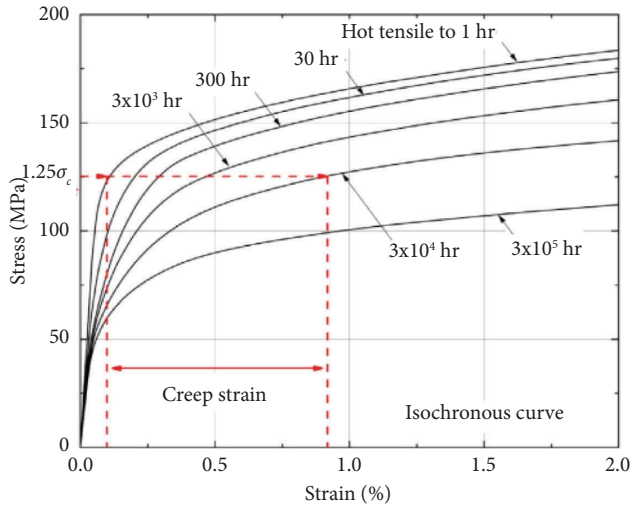

Figure 7: General method of obtaining the creep strain from isochronous curves.

The fatigue-creep damage of the equipment was evaluated according to ASME-NH. Based on the linear cumulative damage method, the fatigue damage caused by the load cycle and the creep damage caused by high-temperature load holding are superimposed as the total damage. The component fails when $D \gg \mathrm{Dcr}$ ($\mathrm{Dcr} = 1$, critical damage). Combined with the creep-fatigue interaction curve, the total damage (D) had to be within the creep-fatigue damage envelope [21]. Therefore, creep and fatigue damage had to satisfy the following equation:

$$\sum_{j=1}^{p}\left(\frac{n}{N_d}\right)_j + \sum_{k=1}^{q}\left(\frac{\Delta t}{T_d}\right)_k \le D. \quad (9)$$

3. Finite Element Analysis

3.1. Geometrical Model and Meshing. The geometrical model and the cross-section of the thin double-layered annulus ZrCo hydride bed are shown in Figure 8. To facilitate finite element meshing based on Saint-Venant's principle [28], the geometric model was reasonably simplified, and certain details such as the threaded holes, chamfers, and small fillets were removed. The simplified model and the specific local details are shown in Figure 9.

The 3D representation of the hydrogen storage bed was obtained, which included inner and outer bed bodies, inner

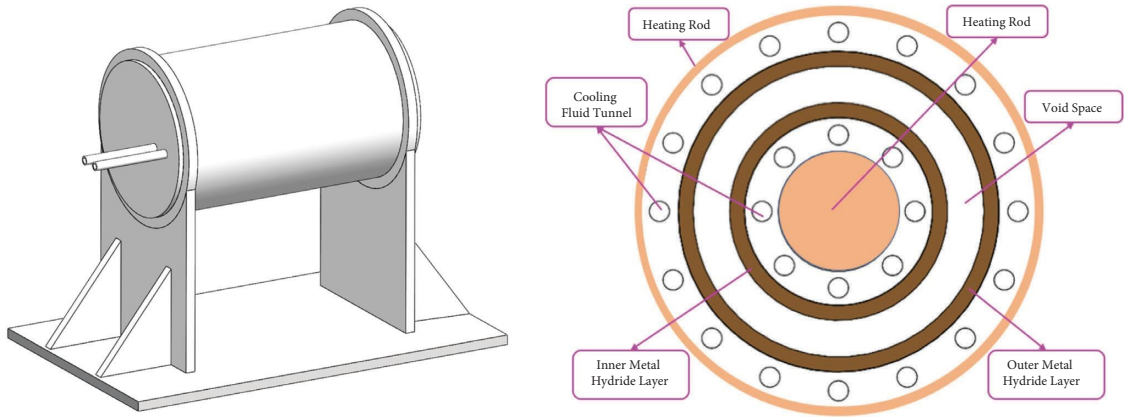

Figure 8: Schematic of (a) geometrical model and (b) cross-section of the thin double-layered annulus bed.

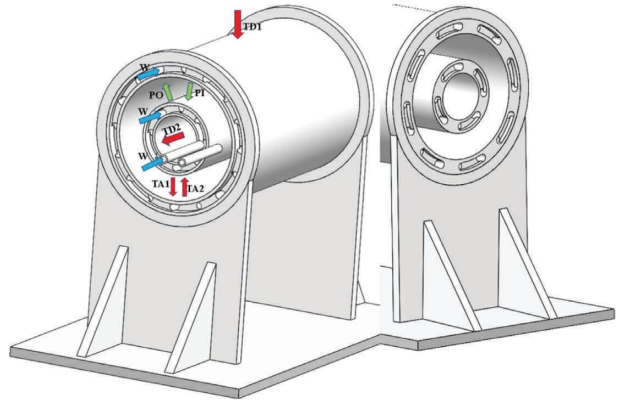

Figure 9: Simplified model and specific local details of the hydrogen storage bed. (w represents water; TA and TD represent the temperature of hydrogen absorption and desorption, respectively; PO and PI represent pressure of outer ring and inner ring of the hydrogen storage bed, respectively).

and outer hydrogen storage layers, and inner and outer filter layers. There was also a cavity structure between the two stainless steel filter cartridges, which contained a gas layer for the flow of the hydrogen isotope gas. The cavity was connected to the inlet and outlet pipes of the system. In addition, there were M-type cooling medium circulation loops drilled along the length direction on the inner and outer stainless steel bed body walls, which could be used for rapid cooling of the bed body or flow-gas calorimetry when storing tritium.

In this study, the hydrogen storage bed structure materials are all composed of 316L stainless steel. The physical properties of 316 stainless steel are shown in Table 1. The overall finite element meshing of the hydrogen storage reactor structure is shown in Figure 10. Tetrahedral and hexahedral grids were used for different components of the hydrogen storage bed, according to their geometry and complexity. The mesh quality was also maintained at a reasonable level to ensure a high computational speed. A total number of 1382202 elements and 2078936 nodes were generated in this model.

3.2. Thermal and Structural Loads Analysis. When the hydrogen storage layer absorbs hydrogen, a large amount of heat is released instantaneously, and the temperature of the hydrogen storage layer rapidly rises from room temperature to 200 degrees. In order to improve the hydrogen absorption efficiency, the hydrogen storage bed is cooled by passing cooling water. The temperature evolution history of the hydrogen storage layer during the hydrogen absorption process is shown in Figure 11.

Generally speaking, the higher the temperature, the higher the hydrogen release platform of the hydrogen storage material, the faster the hydrogen release kinetics, and the easier it is to release hydrogen quickly. However, since ZrCo alloy is very easy to disproportionate when the temperature is higher than 500°C and the hydrogen pressure is high than 0.5 bar, the hydrogen desorption rate and disproportionation effect should be comprehensively considered in the selection of the hydrogen desorption temperature of the ZrCo bed. Therefore, the dehydrogenation temperature of the ZrCo bed should be strictly controlled below 500°C, and the hydrogen pressure should be controlled below 1 MPa. The

Table 1: Physical properties of 316 ss [29].

Temperature (K)	Specific heat (J/kg/K)	Thermal conductivity (w/m/K)	Thermal expansion (10^{-6} m/m/K)	Young's modulus (10^{11} Pa)	Poisson's ratio	Density (kg/m^3)
273	492	14.12	14.56	1.956		
283	502	15.26	15.39	1.912		
473	514	16.69	16.21	1.857	0.294	7966
673	538	19.54	17.37	1.726		
1073	562	22.38	18.12	1.550		

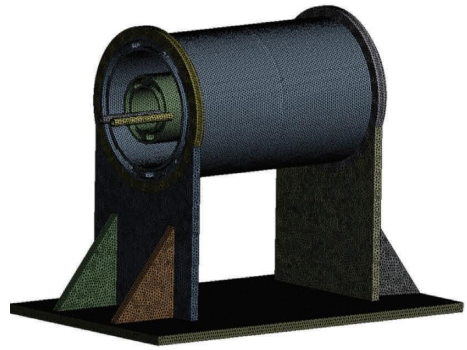

Figure 10: Overview of tube meshes of hydrogen storage beds.

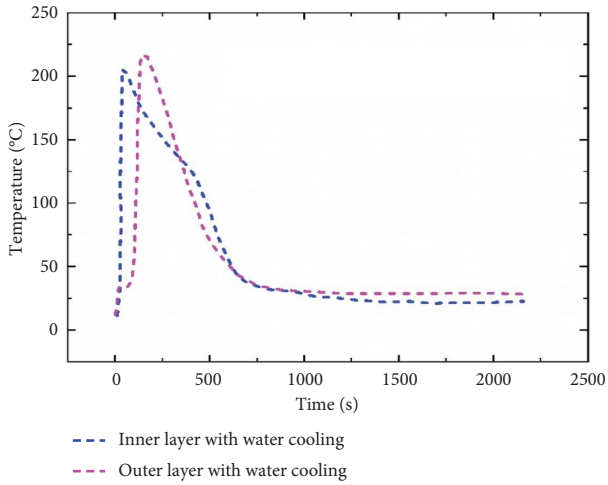

Figure 11: Temperature evolution of ZrCo bed with cooling water during hydrogen absorption.

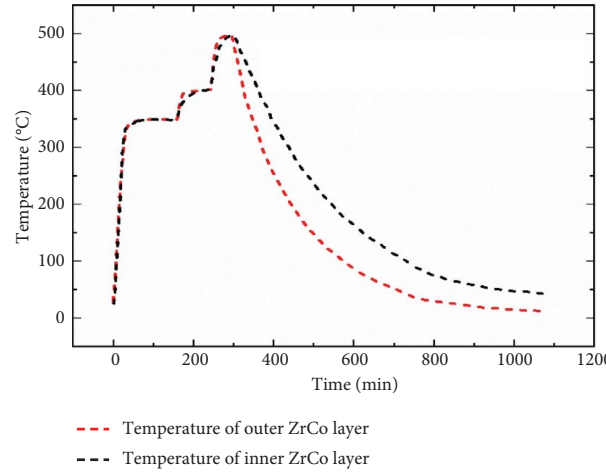

Figure 12: Temperature evolution history of ZrCo bed during hydrogen desorption.

temperature change of the hydrogen storage layer during hydrogen desorption is shown in Figure 12.

The calculated loads include self-weight, internal pressure, and heat load changes in the hydrogen absorption and desorption processes. In the hydrogen absorption and exothermic stage, the heat load is generated in the inner and outer hydrogen storage layers, and the cooling pipe is cooled by water. In the hydrogen desorption and endothermic stage, the internal heating rod and the external heating shell are used for heating. The peak and valley load conditions of the corresponding parts of the hydrogen storage bed structure in the process of hydrogen absorption and desorption are shown in Table 2.

4. Result Analysis and Discussion

4.1. Stress Characteristics Analysis

4.1.1. Stress Distribution. In the hydrogen absorption process, the hydrogen storage layer is accompanied by exothermic phenomenon. In order to increase the hydrogen absorption rate, the cooling system is activated to take away heat; the hydrogen desorption process is an endothermic reaction. The temperature distribution of the main body of the hydrogen storage bed under the two working conditions is shown in Figure 13. It can be seen from figure that the cooling pipe system greatly affects the temperature distribution of the hydrogen storage bed. The geometric structures of the two ends of the hydrogen storage bed are

Table 2: Loads conditions of the hydrogen absorption and desorption process.

Process	Temperature (K)	Pressure (MPa)
Hydrogen absorption	TA = TA1 & TA2 = 473.15 K TW = 295.15 K	PO & PI = 1 MPa
Hydrogen desorption	TD = TD1 = TD2 = 873.15 K TA = TA1 = TA2 = 773.15 K	PO & PI = 0.6 MPa

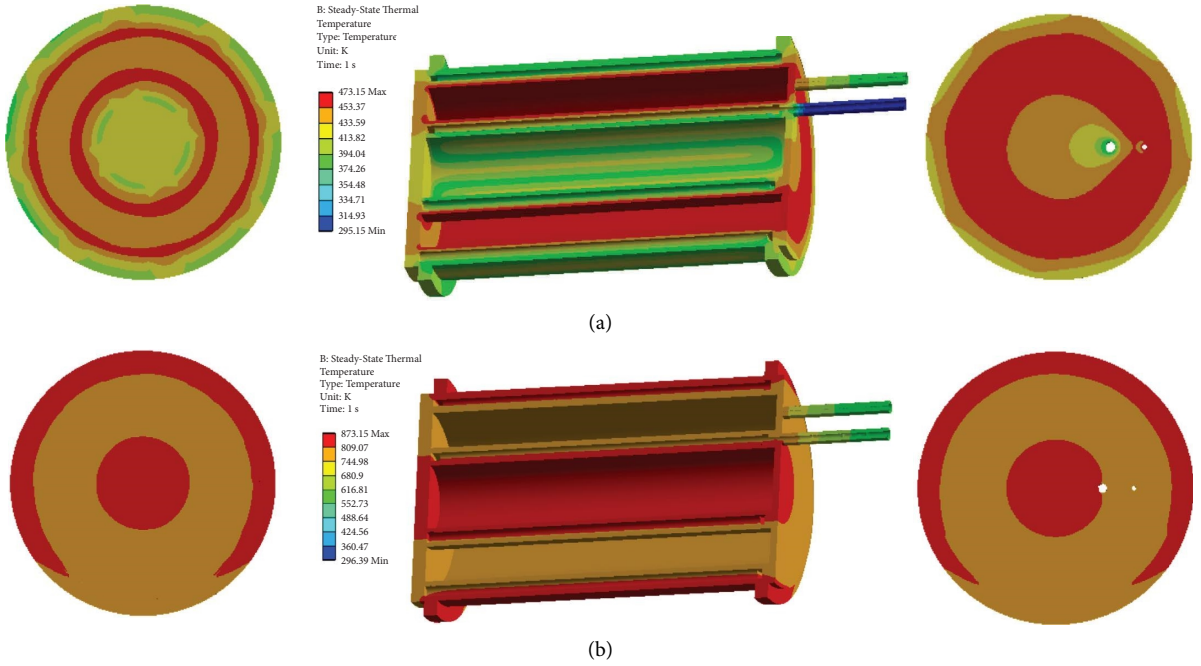

Figure 13: The system temperature contour of (a) hydrogen absorption process and (b) hydrogen desorption process.

different. During the hydrogen absorption process, the temperature distribution is affected by the cooling system on one side as a "petal shape" and on the other side as a "flame shape," while the geometric structure in the hydrogen release stage has little effect.

It is difficult to determine the heat transfer coefficient between W and the walls of the hydrogen storage bed structure under the hydrogen absorption condition. According to Mechanical User's Guide of ANSYS soft, in the convection part of boundary condition setting, we set the ambient temperature for numerical simulation as 295.15 K and obtained the heat exchange coefficient of 1200 $W/m^2 \cdot K$ by importing convection data with water as the fluid. At the same time, in order to ensure the reliability of heat transfer coefficient, the heat transfer coefficient between W and the wall of hydrogen storage bed is also calculated by Liu and Winterton's correlation [30]. The calculation result is also close to that in design condition. Therefore, the heat transfer coefficient in design condition is adopted to investigate the stress distribution of hydrogen storage bed structures. The working conditions of the hydrogen absorption and desorption process are shown in Table 1, and the stress distribution under the two working conditions is shown in Figure 14. It can be seen from figure that the maximum stress of the thermal-structure coupling during the hydrogen absorption process occurs about 1/3 along the diameter direction and at the geometrical abrupt change of the connection between the cooling pipe and the main body of the hydrogen storage bed during the hydrogen desorption process. The hydrogen absorption-desorption cycle of the hydrogen storage bed is affected by many factors. In order to further understand the stress phenomenon in the hydrogen absorption and desorption process of the hydrogen storage bed, we need to study the influence rules of these factors.

4.1.2. Effect of Temperature Difference on Stress. During the hydrogen absorption and desorption process of the hydrogen storage bed, the temperature difference between TA and TW during the hydrogen absorption process is different, resulting in different stress states of the hydrogen storage bed. In order to understand the effect of temperature difference on the safety and stability of the hydrogen storage bed structure, the thermal stress distribution under different temperature differences between TA and TW was analyzed. Figure 15 shows the equivalent stress peaks for different temperature differences and different heat transfer coefficients at the temperature of 295.15 K of W. The results show that the peak value of equivalent stress increases with the increase of the temperature difference, and the temperature difference has a significant effect on the stress of the hydrogen storage bed structure. The heat transfer coefficient between W and the walls of the hydrogen storage bed has a great influence on the stress of the hydrogen storage bed. The larger the heat transfer coefficient, the greater the effect of the temperature difference on the stress of the hydrogen

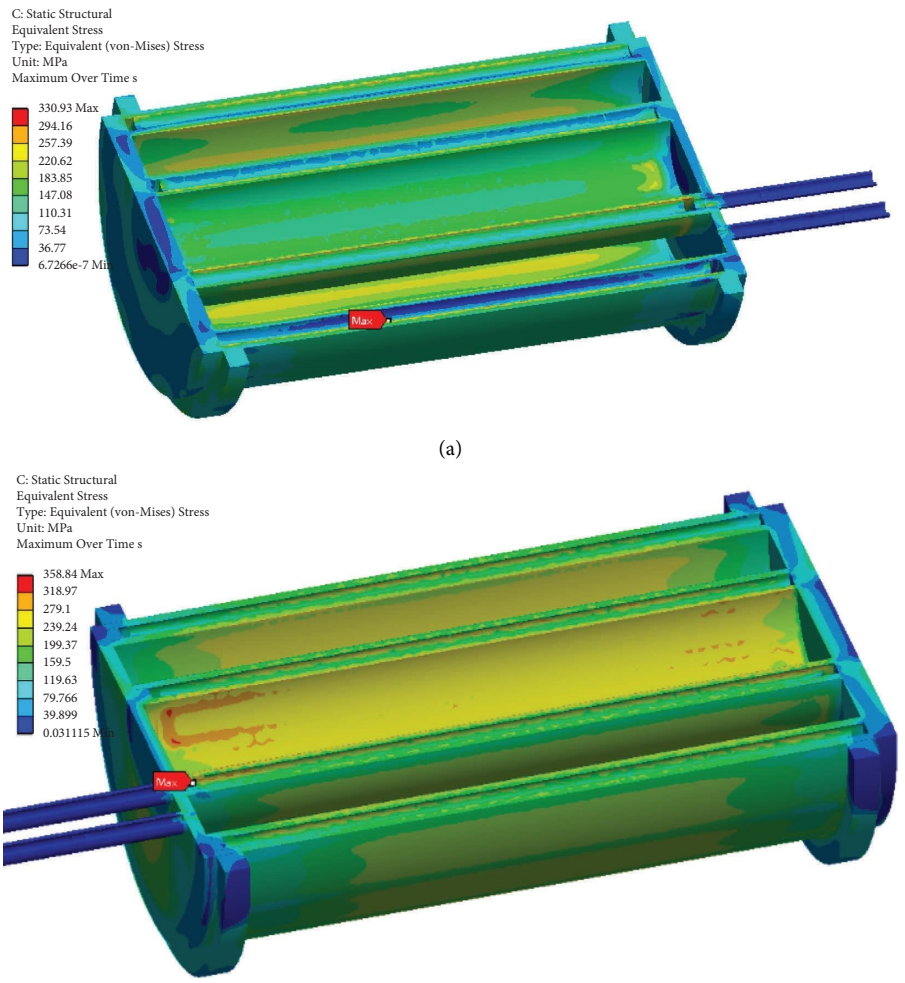

Figure 14: Equivalent stress distribution on hydrogen storage bed during (a) absorption process and (b) desorption process.

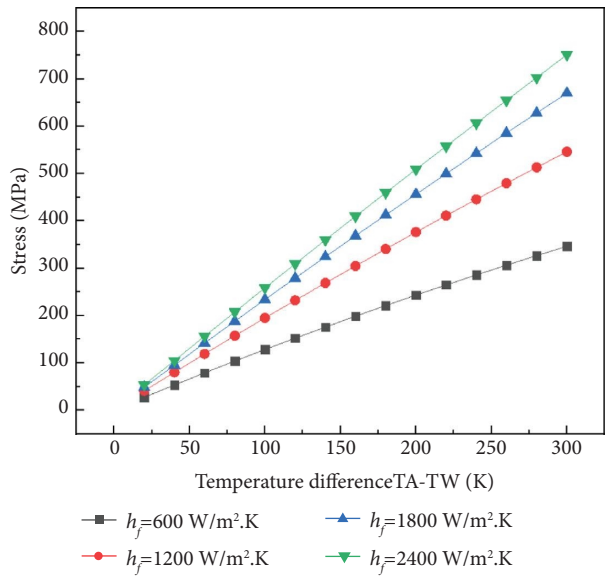

Figure 15: The peak value of $\sigma_{\text{von-mises}}$ vs. temperature difference at different heat transfer coefficients.

storage bed. With the increase of the heat transfer coefficient, the effect of the heat transfer coefficient on the temperature difference is smaller.

At the same time, the stress along the length of the cooling tube during the hydrogen absorption and desorption process of the hydrogen storage bed is also different, because the temperature from the W inlet to the outlet is different. Therefore, the effect of temperature difference on stress at different temperatures of W is also analyzed. Figure 16 shows the relationship between the equivalent stress peak value and temperature difference at different TW when the heat transfer coefficient is 1200 W/m^2·K. The results show that with the increase of the temperature difference, the stress peak trend of the hydrogen storage bed is also larger. The peak stress is affected by the TW. When the temperature difference is greater than 200 K, the smaller TW, the greater the peak stress TW can be appropriately increased. When the temperature difference is less than 80 K, the higher the TW, the greater the peak stress, it is better to reduce TW.

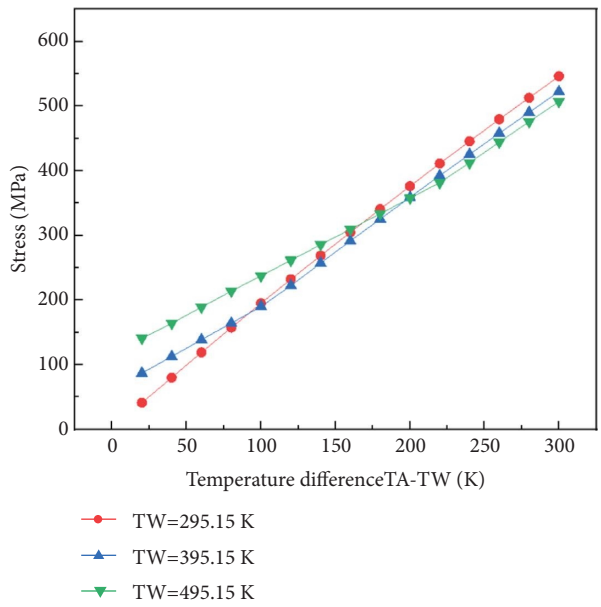

FIGURE 16: The peak value of $\sigma_{\text{von-mises}}$ vs. temperature difference at different W temperature.

4.1.3. Effect of Temperature Change Rate on Stress. The hydrogen absorption process of the hydrogen storage bed is relatively complicated. With the progress of the chemical reaction, there is not only the process of heating and cooling but also the operation of the cooling system to reduce the temperature as soon as possible. Therefore, the effect of temperature rate change on the stress of the hydrogen storage bed can be studied by analyzing the relationship between the rise rate, drop rate, and the equivalent stress peak value. Figures 17 and 18 depict the relationship between the peak value of equivalent stress and the rate of temperature rise and temperature drop under different heat transfer coefficients at the initial temperature of the cooling medium at 295.15 K degrees, respectively. The results show that the rise rate and drop rate have little effect on the stress of the hydrogen storage bed, but it is greatly affected by the heat transfer coefficient. The greater the heat transfer coefficient, the greater the equivalent peak stress. However, as the heat transfer coefficient increases, the degree of influence decreases. At the same time, the peak value of equivalent stress increases with the increase of the rise rate and decreases with the decrease of the drop rate. The reason is that the hydrogen storage bed has excellent heat transfer performance. When TA increases, it has a similar rise rate to W, so it is less affected by the rise rate, but when TA decreases, W is still in a rise state.

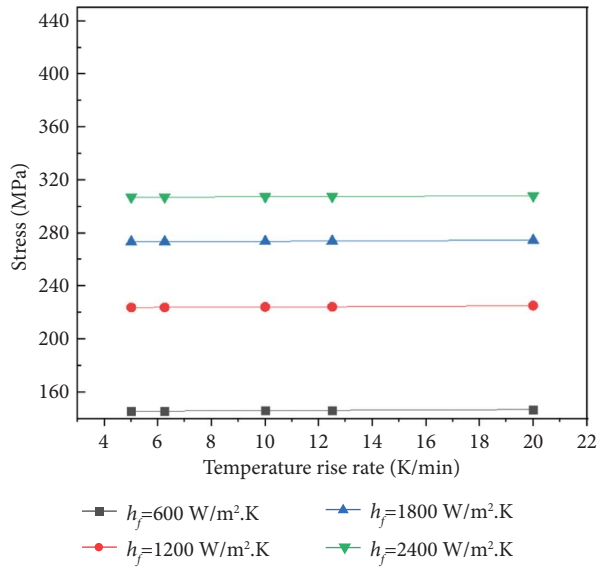

FIGURE 17: The peak value of $\sigma_{\text{von-mises}}$ vs. the temperature rise rate at different heat transfer coefficients.

4.1.4. Effect of Heat Transfer Performance on Stress. The heat transfer performance directly affects the hydrogen absorption-desorption efficiency of the hydrogen storage bed and also affects the stress distribution. The heat transfer coefficient between the coolant and the wall of the hydrogen storage bed is the key parameter of the heat transfer performance of the hydrogen storage bed. Therefore, the relationship between the heat transfer coefficient and the peak equivalent stress of the hydrogen storage bed was studied. Figure 19 depicts the relationship between the equivalent stress peak value and the heat transfer coefficient under different temperature differences. The results show that with the increase of the heat transfer coefficient, the corresponding peak value of equivalent stress also increases gradually, but the growth rate becomes slower and slower, and the trend gradually becomes gentle. However, as the temperature difference increases, the peak stress becomes larger and the corresponding growth rate becomes faster.

4.1.5. Effect of Pressure on Stress. According to the actual working conditions of the hydrogen storage system, the hydrogen storage bed is not only subjected to the hydrogen pressure in the process of hydrogen absorption-desorption

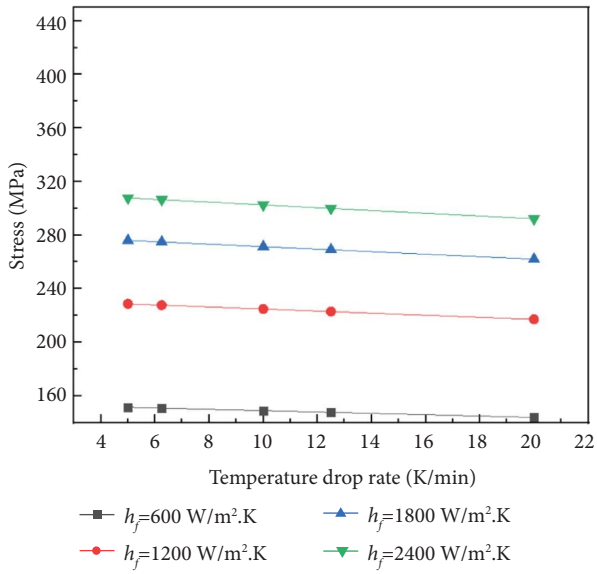

FIGURE 18: The peak value of $\sigma_{\text{von-mises}}$ vs. the temperature drop rate at different heat transfer coefficients.

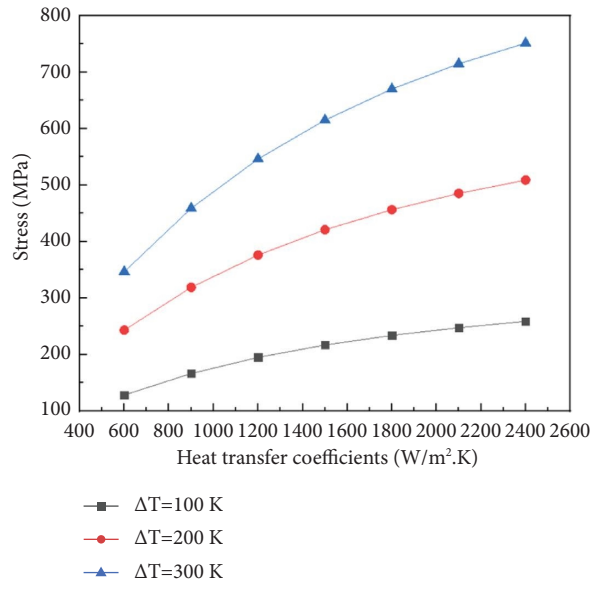

FIGURE 19: The peak value of $\sigma_{\text{von-mises}}$ vs. heat transfer coefficients of W at different temperature difference.

but also the expansion and contraction pressure of the hydrogen storage layer due to the deformation of hydrogen metal. Therefore, the effect of stress on the hydrogen storage bed was analyzed. The pressure is taken as 0.5 bar–200 bar. Figure 20 depicts the relationship between pressure and peak equivalent stress under a temperature difference of 200 K and a heat transfer coefficient of 1200 W/m^2·K. The results show that 1 MPa is a turning point, and the stress curve of the pressure-to-hydrogen storage bed structure first decreases and then increases. From Figure 21, we can see that the reason for the turning after 1 MPa is that the position where the maximum stress occurs in the hydrogen storage bed is

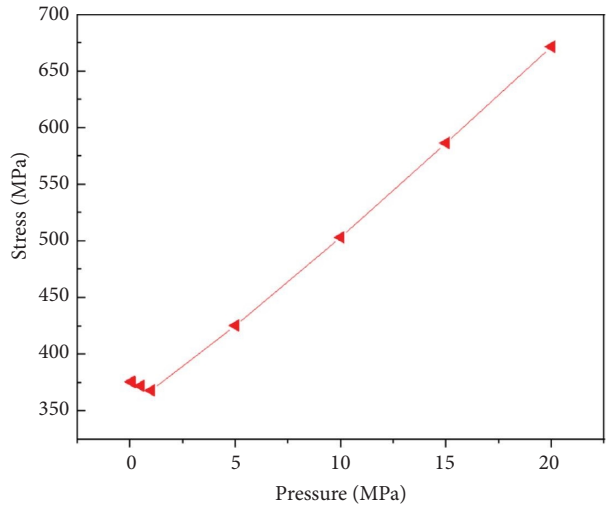

FIGURE 20: The peak value of $\sigma_{\text{von-mises}}$ vs. pressures.

transferred from the inner ring of the hydrogen storage bed to the outer ring. Therefore, in the actual operation of the hydrogen storage bed, it is necessary to comprehensively consider the effect of pressure on the stress of hydrogen storage bed structures in different operation processes.

4.2. Thermal Fatigue and Creep Assessments of the Hydrogen Storage Bed

4.2.1. Thermal Fatigue Assessments by ASME-NB. The maximum stress distribution diagrams under the thermal load and pressure conditions during the hydrogen absorption are shown in Figures 22 and 23, respectively. Based on the abovementioned stress distribution results, path A-A and path B-B along the wall thickness were selected for evaluation based on the location of maximum stress. Since the maximum temperature of the hydrogen storage bed in the hydrogen absorption process was lower than 427°C, the ASME-NB standard [20] is used for evaluation. When the low temperature parts are averaged, the primary film stress intensity used was the time-independent allowable stress S_m according to ASME BPVC II-D [31].

The stress linearization results showed that the membrane, bending, and secondary stress values were all within the allowable values of the design stress intensity of the ASME code. The maximum cumulative use factor for 10,000 cycles was 0.0329, which showed that the temperature was relatively low and thermal fatigue was small. The results are shown in Table 3, and Table 4 evaluates the cumulative use factors.

4.2.2. Thermal Fatigue and Creep Assessments by ASME-NH. Creep fatigue assessment is an important part of structural integrity assessment at elevated temperatures. To analyze the stress and deformation levels of the hydrogen storage bed under complex loads, the creep and fatigue damage levels were calculated at key locations, and the total damage of the

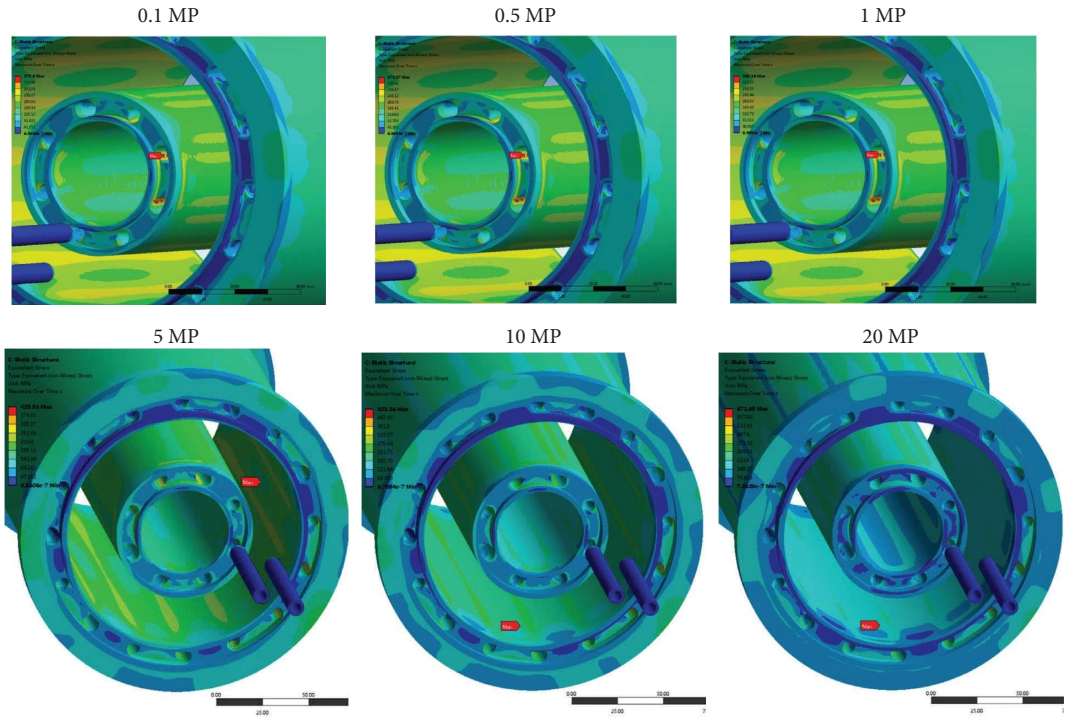

Figure 21: Peak equivalent stress under different pressures.

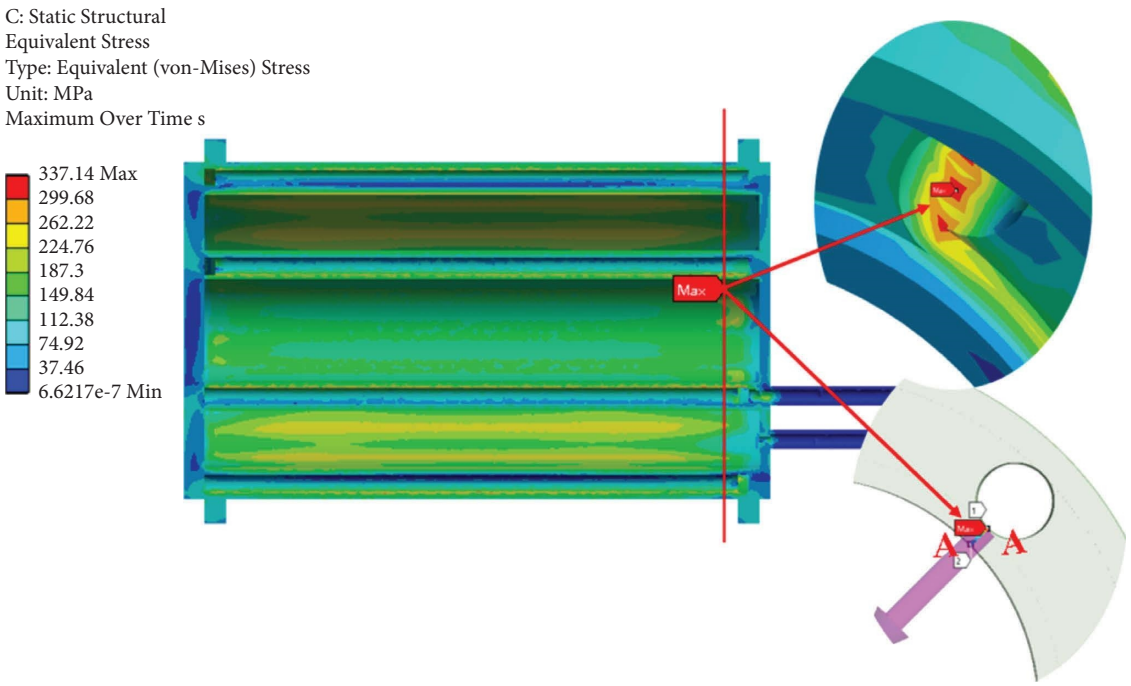

Figure 22: Maximum stress under thermal load.

equipment during the service period should not exceed the creep-fatigue damage envelope of the material. Since the hydrogen storage bed temperature can be up to 500°C in the hydrogen desorption process, the evaluation standard followed the NH Appendix NH-T procedure.

The maximum stress distribution diagrams under the thermal load during the hydrogen desorption are shown in Figure 24. The maximum stress under pressure-only loading is the same as in Figure 25, where the two paths as C-C and D-D were evaluated. Conservative evaluations were carried

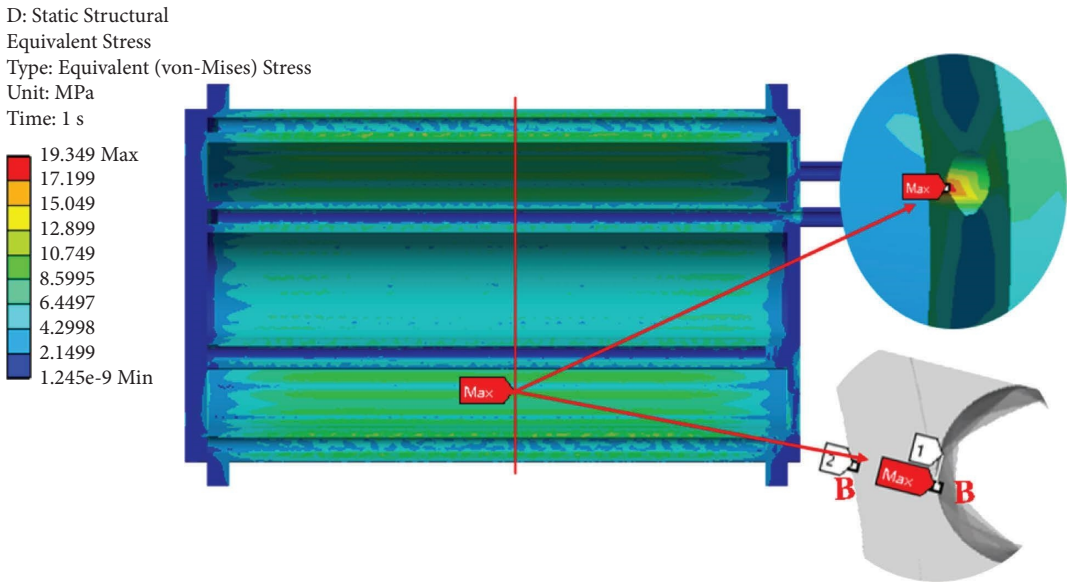

Figure 23: Maximum stress under an internal pressure of only 1 MPa.

Table 3: Evaluation of stress strength and fatigue.

Evaluation item	Code criterion	Evaluation location	Calculated value	Allowable	Check
Stress limits (MPa)	P_L	A-A	7.55	109	Ok
		B-B	10.16		Ok
	$P_L + P_b$	A-A	9.54	164	Ok
		B-B	16.51		Ok
	$P + Q$	A-A	239.09	327	Ok
		B-B	113.43		Ok
Fatigue limit	Cumulative usage factor		0.059	1.0	Ok

Table 4: Evaluation procedure of the cumulative usage factor.

Fatigue event	Service conditions: Heating and cooling process Design cycles: 10,000 cycles
The selected location for fatigue evaluation	Two locations are selected where the maximum stress occurs
Design fatigue curve	Fig. I-9-2.2: ASME sec. III, div. 1, appendix I $P + Q$ stress intensity range = 239.09 MPa
Fatigue evaluation	Alternating stress intensity = 165.47 MPa Allowable number: 169560 cycles Cumulative usage factor = 0.059

out according to the A-level service limit, and elastic analysis and inelastic analysis were used to check whether the strain limit in the high temperature area was satisfied.

In the evaluation of high temperature components, two variables are introduced; St and S_{mt}, where St is the stress intensity related to time and temperature and S_{mt} is the average stress of high temperature components during the actual service period. The effective creep stress parameter Z was obtained by a linear interpolation from the simplified inelastic analysis in the literature test B-2, and the effective creep stress σ_c was achieved. Finally, the creep ratchet strain $\Delta\varepsilon_c$ (%) can be obtained corresponding to 1.25 σ_c from the isochronous stress-strain curve.

According to equation (2), the maximum strain range $\Delta\varepsilon_{\max}$ considered the stress concentration effect caused by the discontinuity of the geometric structure. The parameters required to calculate the total strain range $\Delta\varepsilon_t$, which corresponded to the linear interpolation of the fatigue design

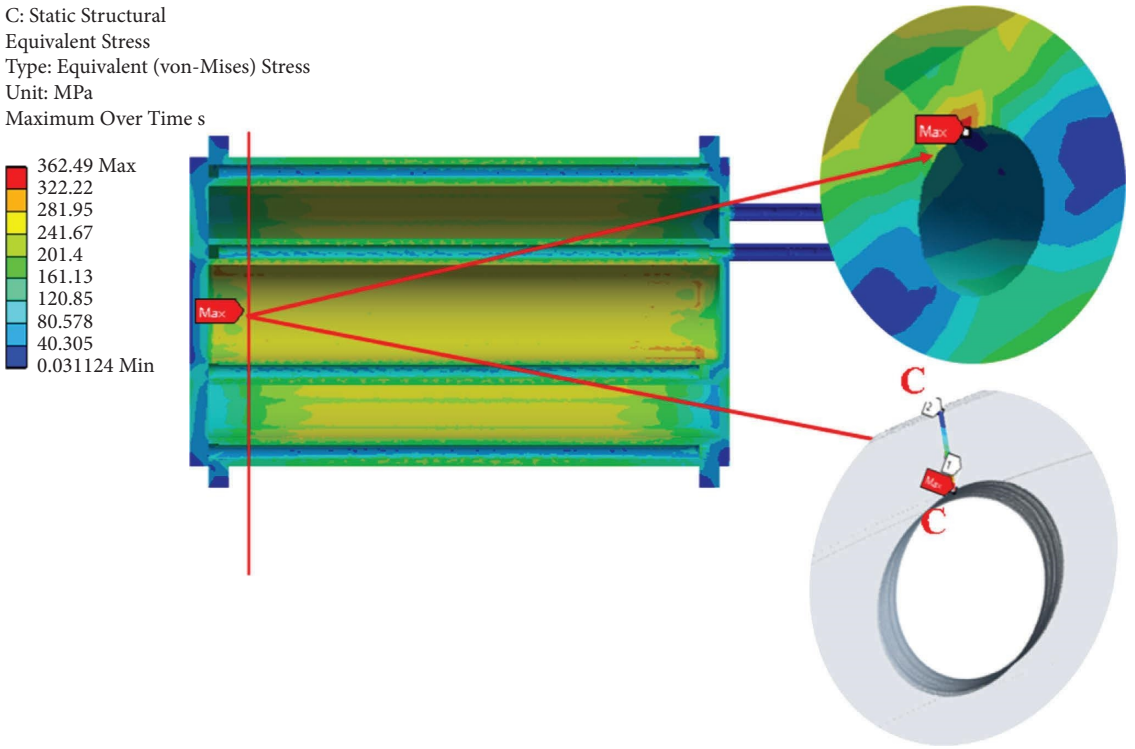

Figure 24: Maximum stress under thermal load.

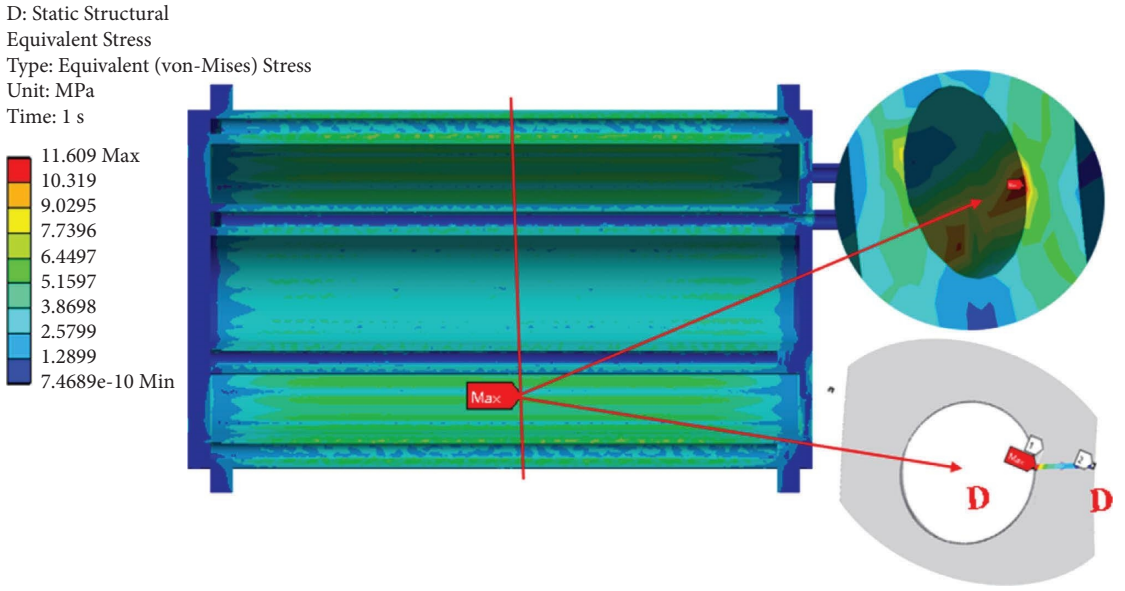

Figure 25: Maximum stress under internal pressure of only 0.6 MPa.

Table 5: Parameters for creep-fatigue damage evaluation.

Path	K	K_e	K_v	Z	$\Delta\varepsilon_{mod}$ (%)	σ_c (MPa)	$\Delta\varepsilon_c$ (%)	$\Delta\varepsilon_t$ (%)	Nd	Td (hr)
C-C	1.0	1.25	1.21	0.5	0.22	60.71	0.16	0.43	3565	3×10^5
D-D	1.0	1.35	1.08	0.4	0.18	48.57	0.08	0.27	18979	3×10^5

Table 6: Evaluation results of thermal fatigue and creep.

Evaluation item		C-C			D-D		
		Calculated value	Limit	Check	Calculated value	Limit	Check
Primary stress limits (MPa)	Membrane	3.22	106	Ok	5.93	106	Ok
	Membrane + bending	5.24	167	Ok	9.80	167	Ok
Inelastic strain limits	Elastic analysis	0.732	1.0	Ok	0.542	1	Ok
	Simplified inelastic analysis	0.000	1%	Ok	0.000	1%	Ok
Creep-fatigue limits	Fatigue damage	0.084	—	—	0.016	—	—
	Creep damage	0.1	—	—	0.1	—	—

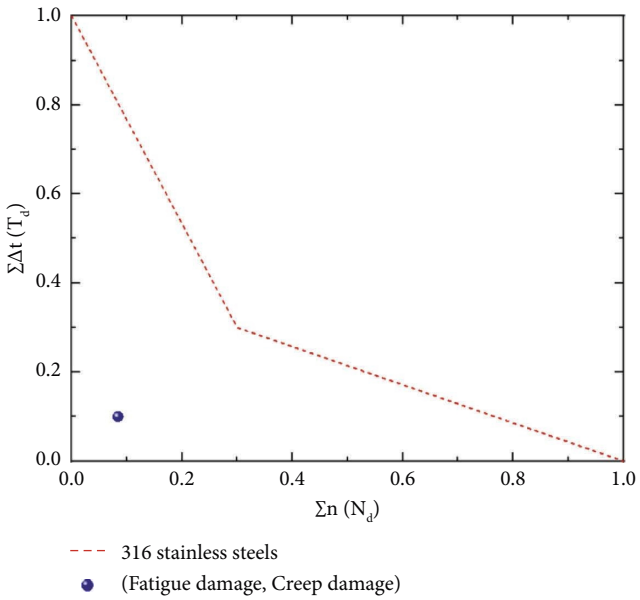

Figure 26: Creep-fatigue damage of the hydrogen storage bed.

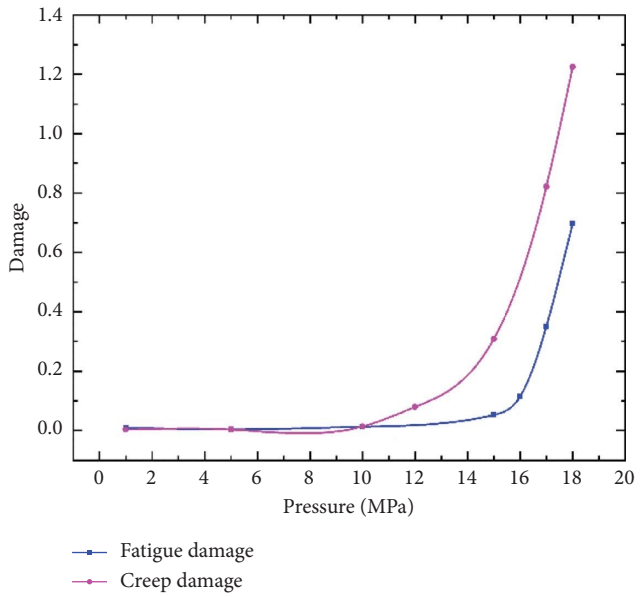

Figure 27: Evolution of creep and fatigue damage with hydrogen pressure.

curve [21], where for ε_t, the allowable number of cycles Nd was obtained. The design life of the hydrogen storage bed was 300.00 hours, and the design start and end cycles is 300. The calculation parameters of fatigue-creep evaluation are shown in Table 5, and the evaluation results are summarized in Table 6.

Based on the abovementioned evaluation results, the accumulated creep damage during the design life was 0.1. Compared to fatigue damage, creep damage occupied a dominant proportion in the structure of the hydrogen storage bed, which was higher than fatigue damage. By not taking into account the effects of stress relaxation in the calculation process, the most dangerous transient conditions were evaluated, and an overly conservative estimate of creep damage was obtained. The creep and fatigue damage accumulated during the service life was within the damage envelope as shown in Figure 26. Thus, the design was ASME-NH-compliant.

4.2.3. Effect of Primary Load on Creep-Fatigue Damage. The pressure affects the hydrogen absorption and desorption efficiency of the hydrogen storage bed and also changes the strain range of the hydrogen storage bed, thereby affecting the creep damage, fatigue damage and life of the hydrogen storage bed. In order to clarify the potential impact mechanism, we studied the fatigue damage and creep damage of the hydrogen storage bed under different pressures, and the specific evolution is shown in Figure 27. From Figure 27, we can see that when the pressure was greater than 12 MPa, the creep damage accelerates, while the fatigue damage increases significantly after 16 MPa.

5. Conclusions

This paper provides an overview of a conform-to-design thermal-structural creep and fatigue analysis of a double-layered annulus metal hydride bed by an analytical approach that considers the ultimate failure mode condition. Based on the analysis method, the effect of operating parameters on the stress of the hydrogen storage bed was studied. Combined with ASME-NB and ASME-NH codes and numerical modeling, the fatigue and fatigue creep of double-layer annular metal hydride bed during hydrogen absorption and

desorption were evaluated respectively. From this study, the following conclusions can be drawn.

(1) The numerical simulation results indicate that the maximum stress of the thermal-structure coupling during the hydrogen absorption process occurs about 1/3 along the diameter direction and at the geometrical abrupt change of the connection between the cooling pipe and the main body of the hydrogen storage bed during the hydrogen desorption process.

(2) The peak value of equivalent stress increases with the increase of the temperature difference, and the temperature difference has a significant effect on the stress of the hydrogen storage bed structure. The larger the heat transfer coefficient, the greater the effect of the temperature difference on the stress of the hydrogen storage bed. When the temperature difference is greater than 200 K, the smaller TW, the greater the peak stress, TW can be appropriately increased. When the temperature difference is less than 80 K, the higher the TW, the greater the peak stress, it is better to reduce TW.

(3) For the hydrogen storage bed structure, the pressure has an obvious effect on the peak stress. The stress curve of the pressure-to-hydrogen storage bed structure first decreases and then increases. The temperature rise rate and drop rate have little effect on the stress of the hydrogen storage bed, but it is greatly affected by the heat transfer coefficient. The greater the heat transfer coefficient, the greater the equivalent peak stress.

(4) A systematic evaluation system for the creep and fatigue of the hydrogen storage bed during the hydrogen absorption and desorption process was established. In the hydrogen storage bed, inelastic strain occurs during the hydrogen desorption process, and significant high temperature creep damage occurs. High temperature is an important factor affecting the structural integrity of the hydrogen storage bed. It was found that the fatigue damage generated during its service life was very small, while the creep damage was relatively large. The accumulated creep and fatigue damage over the service life was within the damage envelope.

Under the premise of designing life, according to the process parameters proposed in this paper, the estimated life under the interaction of creep properties is higher than designing life, and the relationship between process parameters and life is established. In order to improve the operating efficiency of the bed, one can consider giving up the marginal integrity of the heating and cooling rates of the hydrogen storage bed.

Abbreviations

P_m: Primary membrane stress intensity
P_L: Local primary membrane stress intensity
P_b: Primary bending stress intensity
S_y: Averaged yield stress at the maximum and minimum wall temperatures
S_{yL}: Yield stress at the lower of the wall-averaged temperature for extreme stresses
K_t: Parameter accounting for bending
$(Q_R)_{\max}$: Maximum range of secondary stress intensity
N_d: Number of allowable cycles
T_d: Allowable creep rupture time
$\Delta\varepsilon_{\text{mod}}$: Modified maximum strain range
$\Delta\varepsilon_{\text{cr}}$: Creep strain increment in one cycle
$\Delta\varepsilon_{\max}$: Maximum equivalent strain range
$\Delta\varepsilon_t$: Total strain range
X: Primary stress parameter
Y: Secondary stress parameter
Z: Effective creep stress parameter
σ_c: Effective creep stress
K: Local geometric concentration factor
K_v: Multiaxial plasticity and Poisson's ratio adjustment factor.

Data Availability

The raw/processed data required to reproduce the findings in the current manuscript cannot be shared at this time as these data also form a part of an ongoing study.

Conflicts of Interest

The authors declare that they have no conflicts of interest.

Acknowledgments

The authors gratefully acknowledge the financial support of the Basic Research for Application Foundation of Sichuan Province "Study on Dynamic Characteristics and Optimization of Heat and Mass Transfer Process in Metal Hydrogen Storage Bed" (Grant no. 2020YJ0257).

References

[1] N. S. Mustafa, F. A. Halim Yap, M. Yahya, and M. Ismail, "The hydrogen storage properties and reaction mechanism of the NaAlH4 + Ca(BH4)2 composite system," *International Journal of Hydrogen Energy*, vol. 43, no. 24, Article ID 11132, 2018.

[2] H. Yoshida, O. Kveton, J. Koonce, D. Holland, and R. Haange, "Status of the ITER tritium plant design," *Fusion Engineering and Design*, vol. 39–40, pp. 875–882, 1998.

[3] A. Chibani, C. Bougriou, and S. Merouani, "Simulation of hydrogen absorption/desorption on metal hydride LaNi 5 -H 2: mass and heat transfer," *Applied Thermal Engineering*, vol. 142, pp. 110–117, 2018.

[4] S. Shafiee and M. H. McCay, "Different reactor and heat exchanger configurations for metal hydride hydrogen storage systems – a review," *International Journal of Hydrogen Energy*, vol. 41, no. 22, pp. 9462–9470, 2016.

[5] T. Saito, K. Suwa, and T. Kawamura, "Influence of expansion of metal hydride during hydriding–dehydriding cycles," *Journal of Alloys and Compounds*, vol. 253-254, pp. 682–685, 1997.

[6] G. Locatelli, M. Mancini, and N. Todeschini, "Generation IV nuclear reactors: current status and future prospects," *Energy Policy*, vol. 61, no. 10, pp. 1503–1520, 2013.

[7] W. Chen, T. Kitamura, and M. Feng, "Creep and fatigue behavior of 316L stainless steel at room temperature: experiments and a revisit of a unified viscoplasticity model," *International Journal of Fatigue*, vol. 112, pp. 70–77, 2018.

[8] F. Heubner, C. Pohlmann, S. Mauermann, B. Kieback, and L. Rontzsch, "Mechanical stresses originating from metal hydride composites during cyclic hydrogenation," *International Journal of Hydrogen Energy*, vol. 40, no. 32, Article ID 10123, 2015.

[9] K. Nasako, Y. Ito, N. Hiro, and M. Osumi, "Stress on a reaction vessel by the swelling of a hydrogen absorbing alloy," *Journal of Alloys and Compounds*, vol. 264, no. 1-2, pp. 271–276, 1998.

[10] B. Y. Ao, S. X. Chen, and G. Q. Jiang, "A study on wall stresses induced by LaNi5 alloy hydrogen absorption–desorption cycles," *Journal of Alloys and Compounds*, vol. 390, no. 1-2, pp. 122–126, 2005.

[11] L. Dinachandran and G. Mohan, "Numerical simulation of the parametric influence on the wall strain distribution of vertically placed metal hydride based hydrogen storage container," *International Journal of Hydrogen Energy*, vol. 40, no. 16, pp. 5689–5700, 2015.

[12] F. Sen, E. Celik, and M. Toparli, "Transient thermal stress analysis of CeO2 thin films on Ni substrates using finite element methods for YBCO coated conductor," *Materials & Design*, vol. 28, no. 2, pp. 708–712, 2007.

[13] A. Kandil, A. A. El-Kady, and A. El-Kafrawy, "Transient thermal stress analysis of thick-walled cylinders," *International Journal of Mechanical Sciences*, vol. 37, no. 7, pp. 721–732, 1995.

[14] H. Ullah, B. Ullah, and V. V. Silberschmidt, "Structural integrity analysis and damage assessment of a long composite wind turbine blade under extreme loading," *Composite Structures*, vol. 246, Article ID 112426, 2020.

[15] H. G. Kang, S. Cho, M. K. Lee et al., "Fabrication and test of thin double-layered annulus metal hydride bed," *Fusion Engineering and Design*, vol. 86, no. 9-11, pp. 2196–2199, 2011.

[16] S. H. Xu, X. L. Yang, J. Li, B. Shi, and B. Qiu, "The elastic analysis of finite element to the shell of blast furnace under thermal - structural coupling," *Advanced Materials Research*, vol. 368-373, pp. 1495–1499, 2011.

[17] M. S. Patil, J. H. Seo, S. Panchal, and M. Lee, "Numerical study on sensitivity analysis of factors influencing liquid cooling with double cold-plate for lithium-ion pouch cell," *International Journal of Energy Research*, vol. 45, no. 2, pp. 2533–2559, 2020.

[18] Z. Kala, "Sensitivity analysis of the stability problems of thin-walled structures," *Journal of Constructional Steel Research*, vol. 61, no. 3, pp. 415–422, 2005.

[19] K. Yonekura and Y. Kanno, "Second-order cone programming with warm start for elastoplastic analysis with von Mises yield criterion," *Optimization and Engineering*, vol. 13, no. 2, pp. 181–218, 2012.

[20] Asme, "Boiler and pressure vessel code," in *Division 1-Subsection NB*ASME, New York, NY, USA, 2013.

[21] Asme, "Boiler and pressure vessel code," in *Division 1-Subsection NH*ASME, New York, NY, USA, 2013.

[22] X.-L. Yan, X.-C. Zhang, S. T. Tu, S. L. Mannan, F. Z. Xuan, and Y. C. Lin, "Review of creep–fatigue endurance and life prediction of 316 stainless steels," *International Journal of Pressure Vessels and Piping*, vol. 126-127, pp. 17–28, 2015.

[23] W. Chen, T. Kitamura, and M. Feng, "Creep and fatigue behavior of 316L stainless steel at room temperature: experiments and a revisit of a unified viscoplasticity model," *International Journal of Fatigue*, vol. 112, pp. 70–77, 2018.

[24] C. V. Moore, "An introduction to section VIII, division 1 of the ASME boiler and pressure vessel code," *Journal of Pressure Vessel Technology*, vol. 98, no. 3, pp. 231–241, 1976.

[25] G. H. Koo and J. H. Lee, "High temperature structural integrity evaluation method and application studies by ASME-NH for the next generation reactor design," *Journal of Mechanical Science and Technology*, vol. 20, no. 12, pp. 2061–2078, 2006.

[26] J. Bree, "Elastic-plastic behaviour of thin tubes subjected to internal pressure and intermittent high-heat fluxes with application to fast-nuclear-reactor fuel elements," *Journal of Strain Analysis*, vol. 2, no. 3, pp. 226–238, 1967.

[27] N. H. Kim, J. B. Kim, and S. K. Kim, "Development of a structural integrity evaluation program for elevated temperature service according to ASME code," *Nuclear Engineering and Technology*, vol. 53, no. 7, pp. 2407–2417, 2021.

[28] R. A. Toupin, "Saint-Venant's principle," *Archive for Rational Mechanics and Analysis*, vol. 18, no. 2, pp. 83–96, 1965.

[29] X. Ficquet, D. J. Smith, C. Truman, E. Kingston, and R. Dennis, "Measurement and prediction of residual stress in a bead-on-plate weld benchmark specimen," *International Journal of Pressure Vessels and Piping*, vol. 86, no. 1, pp. 20–30, 2009.

[30] Z. Liu and R. H. S. Winterton, "A general correlation for saturated and subcooled flow boiling in tubes and annuli, based on a nucleate pool boiling equation," *International Journal of Heat and Mass Transfer*, vol. 34, no. 11, pp. 2759–2766, 1991.

[31] Amse, *BPVC-IID - 2010 BPVC Section II-Materials-Part D*, ASME, New York, NY, USA, 2010.